ISSN 1674-1056
http://cpb.iphy.ac.cn
http://iopscience.iop.org/cpb
中国物理 B
Chinese Physics
中国物理
Chinese Physics B

# Temperature rise induced by an annular focused transducer with a wide aperture angle in multi-layer tissue

Meng Qi(戚萌), Jiehui Liu(刘杰惠), Yiwei Mao(毛一葳), Xiaozhou Liu(刘晓宙)
**Citation:**Chin. Phys. B . 2018, 27(1): 014301. **doi:** 10.1088/1674-1056/27/1/014301

Journal homepage: http://cpb.iphy.ac.cn; http://iopscience.iop.org/cpb

**What follows is a list of articles you may be interested in**

---

## Nonlinear response of ultrasound contrast agent microbubbles: From fundamentals to applications

Xu-Dong Teng(滕旭东), Xia-Sheng Guo(郭霞生), Juan Tu(屠娟), Dong Zhang(章东)
Chin. Phys. B . 2016, 25(12): 124308. **doi:** 10.1088/1674-1056/25/12/124308

## Low band gap frequencies and multiplexing properties in 1D and 2D mass spring structures

Arafa H Aly, Ahmed Mehaney
Chin. Phys. B . 2016, 25(11): 114301. **doi:** 10.1088/1674-1056/25/11/114301

## Study of the temperature rise induced by a focusing transducer with a wide aperture angle on biological tissue containing ribs

Xin Wang(王鑫), Jiexing Lin(林杰兴), Xiaozhou Liu(刘晓宙), Jiehui Liu(刘杰惠), Xiufen Gong(龚秀芬)
Chin. Phys. B . 2016, 25(4): 044301. **doi:** 10.1088/1674-1056/25/4/044301

## Experimental and numerical studies of nonlinear ultrasonic responses on plastic deformation in weld joints

Yan-Xun Xiang(项延训), Wu-Jun Zhu(朱武军), Ming-Xi Deng(邓明晰), Fu-Zhen Xuan(轩福贞)
Chin. Phys. B . 2016, 25(2): 024303. **doi:** 10.1088/1674-1056/25/2/024303

## Sound field prediction of ultrasonic lithotripsy in water with spheroidal beam equations

Zhang Lue, Wang Xiang-Da, Liu Xiao-Zhou, Gong Xiu-Fen
Chin. Phys. B . 2015, 24(1): 014301. **doi:** 10.1088/1674-1056/24/1/014301

---

# Temperature rise induced by an annular focused transducer with a wide aperture angle in multi-layer tissue*

Meng Qi(戚萌), Jiehui Liu(刘杰惠), Yiwei Mao(毛一葳), and Xiaozhou Liu(刘晓宙)†

*Key Laboratory of Modern Acoustics, Institute of Acoustics and School of Physics, Collaborative Innovation Center of Advanced Microstructures, Nanjing University, Nanjing* 210093, *China*

(Received 22 July 2017; revised manuscript received 4 September 2017; published online 28 November 2017)

In order to improve the operability and accuracy of high-intensity focused ultrasound (HIFU), an annular focused transducer, whereby a B-ultrasound probe is placed in its center, is used to realize the real time monitoring and control of the treatment. In this paper, the spheroidal beam equation (SBE) was used to calculate the sound field by an annular focused transducer with a wide aperture angle to first derive the heat deposition and the Pennes equation was used to calculate the temperature field in multi-layer tissue. We studied the effect of different parameters on the temperature of the tissues. The result shows that the focal length has a significant influence on both maximum liver temperature rise and skin temperature rise, and both increase with the increase in the focal length. When the frequency increases, the temperature rise first undergoes a rapid increase before gradually reaching a maximum, and then finally decreasing. The temperature rise increases while the inner radius decreases or the sound pressure increases. By choosing suitable parameters, the proper temperature rise both on the target tissue and skin via an annular focused transducer with a wide aperture angle can be obtained.

**Keywords:** spheroidal beam equation, annular focused transducer, multi-layer tissue, temperature field

**PACS:** 43.25.+y, 43.80.+p **DOI:** 10.1088/1674-1056/27/1/014301

## 1. Introduction

Biomedical ultrasonics is the study of ultrasound in the biological and medical fields, including ultrasound diagnosis, treatment, and biomedical ultrasound engineering, and has the characteristics of being noninvasive with a high efficiency. High-intensity focused ultrasound (HIFU) is one of the most popular ultrasound surgeries in biomedical ultrasounds. It is not only limited to direct cancer treatment, but has many other applications, such as hemostasis, treatments of ultrasonic lithotripsy, and cardiac conduction.[1–7] The principle of this technique is to use a large ultrasonic focusing transducer to centralize the sound energy on a focal area. A high temperature (above 65 °C) can be achieved in a short period of time and the target tissue undergoes thermal coagulation necrosis, killing the cancerous cells.[8,9]

In recent years, the ultrasound focused field has been widely studied by many researchers. For example, Liu *et al.* used the Khokhlov–Zabolotskaya–Kuznetsov (KZK) equation to study the transmission of finite amplitude sound beams in multi-layered biological media.[10] Li *et al.* used the KZK equation to calculate the influence of the ribs on the sound field.[11] Kamakura *et al.* employed an ellipsoidal coordinate system to develop the spheroidal beam equation (SBE) based on the Westervelt Equation[12] and Lin *et al.* utilized the SBE equation to calculate the sound field in biological tissue with ribs.[13] Meanwhile, the temperature field induced by the focused ultrasound has also been analyzed for many cases. Liu *et al.*[14] studied the temperature field based on the study of Li *et al.*[11] Wang *et al.* examined the influence of the ribs by focusing a transducer with a wide aperture angle on the temperature field.[15] Owing to the potential ability to increase the HIFU efficiency, schemes to improve the blood dissolution and tissue ablation rates have been considered. For example, multi-frequency HIFU is able to improve the rates, especially for large gaps in the different frequencies.[16,17]

As a possible tumor therapy option, HIFU has been extensively studied for several decades. However, there are still many problems waiting to be solved. Owing to the speed of the temperature rise, the offset of the sound focal position and position of the maximum temperature rise are difficult to control, limiting the development and clinical applications of HIFU. In order to realize real-time monitoring and improve the clinical utility, an annular focused transducer with a B-ultrasound probe placed in its center can be used. Kujawska *et al.* designed an annular HIFU transducer and concentrated on the position of the thermal necrosis.[18] Zhang *et al.* used the Rayleigh integral formula to calculate the sound field and then used Pennes bioheat equation to calculate the temperature field of an annular focused ultrasonic transducer. They explored the relationship of the size and shape of the heated

*Project supported by the National Key Research and Development Program, China (Grant No. 2016YFF0203000), the National Natural Science Foundation of China (Grant Nos. 11774167 and 61571222), the Fundamental Research Funds for the Central Universities, China (Grant No. 020414380001), the State Key Laboratory of Acoustics, Chinese Academy of Sciences (Grant No. SKLA201609), and AQSIQ Technology Research and Development Program, China (Grant No. 2017QK125).

†Corresponding author. E-mail: xzliu@nju.edu.cn

© 2018 Chinese Physical Society and IOP Publishing Ltd 

necrosis element with the exposure dose determined by the sound intensity and exposure time.[19]

In this paper, we analyzed the temperature field of an annular focused transducer with a wide aperture angle in multi-layer biological tissue. We first used the SBE to calculate the sound field produced by an annular focused transducer with a wide aperture angle to obtain the heat deposition. The Pennes bioheat equation was then solved to obtain the temperature field in a multi-layer biological tissue including an analysis of several parameters with a dependence on the obtained temperature field.

## 2. Theory

The KZK equation is used to calculate the sound field of an ultrasound transducer based on a parabolic approximation and therefore is only suitable for a transducer with a half-aperture angle $< 16.6^\circ$ (half of the aperture angle of the transducer). A focused transducer with a wide aperture angle is a spherical-shell focused transducer with a spherical half-angle $> 16.6^\circ$.[8] Compared with a small aperture angle focused transducer, a focused transducer with a wide aperture angle has a much better focusing effect and smaller radiating area. Owing to these properties, the focal region, such as tumor tissue, exhibits a higher temperature rise while the other regions experience a lower temperature rise.[20]

The focused transducer with a wide aperture angle can be modeled with the SBE equation. Figure 1 shows the model of our numerical calculations where $a_1$ is the geometric outer radius of focused transducer radiating surface, $a_2$ is the geometric inner radius of the focused transducer radiating surface, $r$ is the focus distance of the transducer, $r_1$ is the thickness of the skin, $r_2$ is the thickness of fat, and $r_3$ is the thickness of the liver. When we calculated the sound field using an annular focused transducer, the initial sound pressure of the inner radius of the focusing transducer corresponding area was zero, while that of the other areas were normal. The calculation method for the sound and temperature fields is presented below.

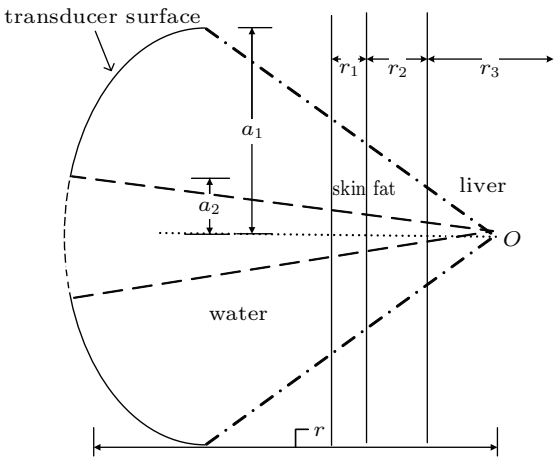



**Fig. 1.** Model for the numerical calculations.

Kamakura *et al.* divided the sound field into spherical and plane wave areas.[10] When $\sigma < \sigma_0$, the area is a spherical wave area because it is close to the surface of the focused transducer. Conversely, the area for is a plane wave area because it is close to the focal point.[21,22] $\sigma_0$ is a critical point.

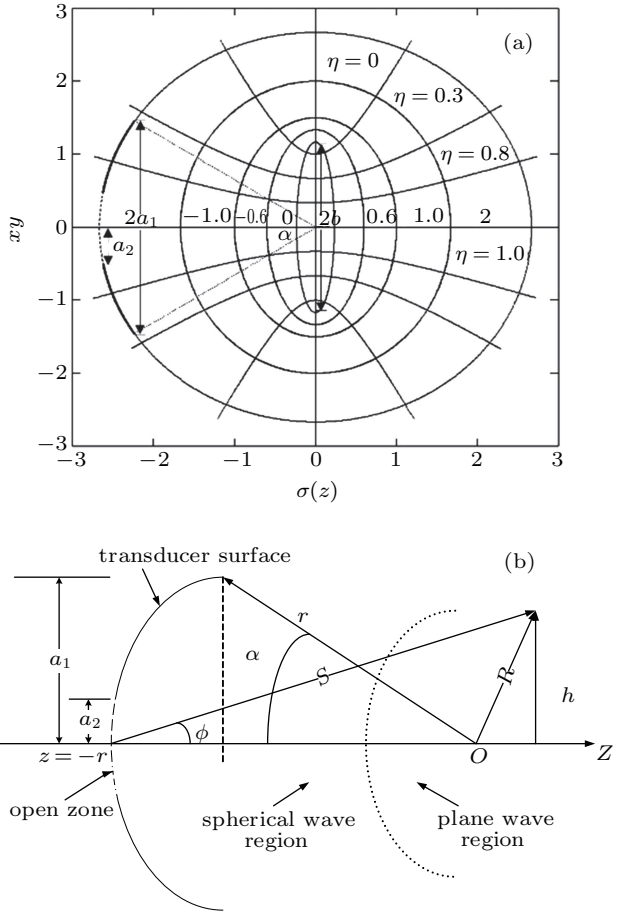



**Fig. 2.** Diagram of the (a) ellipsoidal coordinate system and (b) division of the sound field.

Figure 2 shows the diagram of the ellipsoidal coordinate system, where $\alpha$ is the half-angle of the transducer and 2b is the distance between two focal points of the ellipsoidal coordinate system. The horizontal axis represents the $z$ axis in the $\sigma$ direction. The plane of the vertical axis represents the $x$–$y$ plane. The ellipsoidal coordinates are $(\sigma, \eta, \varphi)$ and $\sigma = z = 0$ is at the geometrical focus. In Fig. 2, $R$ is the distance between any point in the space and the focus, $h$ is the distance between any point in the space and the $z$ axis, and S is the distance between any point in the space and the surface of the transducer.

Using the ellipsoidal coordinate system to calculate the sound field, the relationship between the coordinates of the oblate spheroidal coordinate system $(\sigma, \eta, \varphi)$ and the coordinates of the rectangular coordinate system $(x, y, z)$ is[13]

$$x = b\sqrt{(1+\sigma^2)(1-\eta^2)}\cos\varphi,$$
$$y = b\sqrt{(1+\sigma^2)(1-\eta^2)}\sin\varphi, \quad z = b\sigma\eta, \qquad (1)$$

where $-\infty < \sigma < +\infty$, $0 \le \eta \le 1$, and $0 \le \varphi \le 2\pi$. To simplify the numerical calculation we introduce $\eta = \cos\theta$, where $\theta$ is the included angle between the projection at the $x$–$z$ plane of the connection line between any point of the coordinate system and $x$ axis.

The Westervelt equation can be written as follows:[8]

$$\nabla^2 p - \frac{1}{c_0^2}\frac{\partial^2 p}{\partial t^2} + \frac{\delta}{c_0^4}\frac{\partial^3 p}{\partial t^3} = -\frac{\beta}{\rho_0 c_0^4}\frac{\partial^2 p^2}{\partial t^2}, \tag{2}$$

where $p$ is sound pressure, $\beta$ is the nonlinear coefficients of the medium, $\rho_0$ is the density of the medium, $c_0$ is the sound speed of the medium, $\delta$ is sound diffusion rate, and $t$ is the time. Using a different accompanied coordinate expression we further simplified Eq. (2)

$$\frac{\partial^2 \bar{p}}{\partial\sigma\partial\tau} + A\frac{\partial^2 \bar{p}}{\partial\tau\partial\theta} + B\left(\frac{\partial^2 \bar{p}}{\partial\theta^2} + \cot\theta\frac{\partial \bar{p}}{\partial\theta}\right) + C\frac{\partial \bar{p}}{\partial\tau} = D\alpha\frac{\partial^3 \bar{p}}{\partial\tau^3} + \frac{D}{2l_{\mathrm{D}}}\frac{\partial^2 \bar{p}^2}{\partial\tau^2}, \tag{3}$$

$$\begin{cases} A = \dfrac{\sin 2\theta}{2\sigma(1+\sigma^2)}, \\ B = \dfrac{\varepsilon\sqrt{\sigma^2+\sin^2\theta}}{\sigma(1+\sigma^2)}, \\ C = \dfrac{E}{\sigma}, \\ D = \dfrac{-bE\sqrt{\sigma^2+\sin^2\theta}}{\sigma}, \end{cases} \quad \sigma < \sigma_0 < 0,$$

$$\begin{cases} A = \dfrac{-\sigma\sin\theta}{1+\sigma^2}, \\ B = \dfrac{-\varepsilon(2-\cos\theta)}{1+\sigma^2}, \\ C = 0, \\ D = bE, \end{cases} \quad \sigma > \sigma_0, \tag{4}$$

where $\bar{p} = p/p_0$ is the normalized sound pressure, $p_0$ is the initial pressure, $k = 2\pi\mathrm{f}/c_0$ is the wave number, $f$ is the frequency of the transducer, $\varepsilon = 1/2kb$, $\omega = 2\pi f$, $\alpha = \delta\omega^2/2c_0^3$ is the sound attenuation coefficient, $l_{\mathrm{D}} = \rho_0 c_0^3/\beta p_0\omega$ is the shock formation distance for a planar wave, and:

$$\tau = \omega(t + b\sqrt{1+\sigma^2-\eta^2}/c_0), \quad E = \frac{\sigma^2+\cos^2\theta}{1+\sigma^2}.$$

The normalized sound pressure is subjected to the Fourier decomposition

$$\bar{p} = \sum_{n=-\infty}^{\infty} C_n \mathrm{e}^{-\mathrm{i}n\tau} \approx \sum_{n=-N_{\max}}^{N_{\max}} C_n \mathrm{e}^{-\mathrm{i}n\tau}, \tag{5}$$

where $C_n$ is the $n$-th complex amplitude of a harmonic wave, and $C_{-n} = C_n^*$ denotes the complex conjugate of $C_n$

$$\frac{\partial C_n}{\partial\sigma} = -A\frac{\partial C_n}{\partial\theta} - \frac{\mathrm{i}B}{n}\left(\frac{\partial^2 C_n}{\partial\theta^2} + \cot\theta\frac{\partial C_n}{\partial\theta}\right) - [C + Dn^2\alpha(nf_0)]C_n - \frac{\mathrm{i}nD}{2l_{\mathrm{D}}}\sum_{k=-N_{\max}}^{N_{\max}} C_k C_{n-k}. \tag{6}$$

The relationship between the sound absorption coefficient and frequency is

$$\alpha(nf) = \alpha_*(nf/f_*)^{\mu}, \tag{7}$$

where $\alpha_*$ is the sound absorption coefficient of the medium for a frequency $f_*$, and the value of $\mu$ is 2 in water and 1.1–1.3 in biological tissue. Then we solve Eq. (6) to obtain the sound field.

The heat deposition can be expressed as

$$Q_{\mathrm{v}} = 2\alpha I, \tag{8}$$

where $I = I_0 4\sum_{n=1}^{N_{\max}} |C_n|^2$ and $I_0 = p^2/\rho_0 c_0$ is the sound intensity of the source.

The Pennes bioheat equation[23] can be written as

$$\rho_0 c_{\mathrm{t}}\frac{\partial T}{\partial\tau_{\mathrm{h}}} = K_{\mathrm{t}}\nabla^2 T - w_{\mathrm{b}}c_{\mathrm{b}}(T - T_{\mathrm{b}}) + Q_{\mathrm{m}} + Q_{\mathrm{v}}, \tag{9}$$

where $c_{\mathrm{t}}$ is the specific heat capacity of the tissue, $\tau_{\mathrm{h}}$ is the heat-up time, $K_{\mathrm{t}}$ is the heat conduction coefficient of the tissue, T is the temperature of the tissue, $\omega_{\mathrm{b}}$ is the blood flow rate in the heating area, $c_{\mathrm{b}}$ is the specific heat capacity of blood, $T_{\mathrm{b}}$ is the temperature of the blood in the heating area, $Q_{\mathrm{m}}$ is the heat generation rate of tissue, and $Q_{\mathrm{v}}$ is the heat generation rate of the space heat source.

As the tissue is studied in vitro, $\omega_{\mathrm{b}}$ and $Q_{\mathrm{m}}$ can be ignored. Therefore $Q_{\mathrm{v}}$ is the only source of heat. The Pennes equation[23] can therefore be written as:

$$\rho_0 c_{\mathrm{t}}\frac{\partial \overline{T}}{\partial\tau_{\mathrm{h}}} = K_{\mathrm{t}}\nabla^2\overline{T} + Q_{\mathrm{v}}, \tag{10}$$

where $\overline{T} = T - T_0$ and $T_0$ is the temperature before heating.

## 3. Numerical calculations and analysis

In this chapter we present the numerical calculations of the temperature field by an annular focused transducer. Tables 1 and 2 show the parameters of the relevant biological tissues used in the simulation.

**Table 1.** Sound field parameters.[24,25]

| Medium | $\rho_0$/kg·m$^{-3}$ | $c_0$/m·s$^{-1}$ | $\alpha_*$/Np·m$^{-1}$·MHz$^{-1}$ | $\beta_0$ | $\mu$ |
|---|---|---|---|---|---|
| Water | 1000 | 1500 | 0.0253 | 3.50 | 2.00 |
| Skin | 1090 | 1530 | 11.53 | 4.50 | 2.00 |
| Fat | 910 | 1430 | 9.00 | 10.50 | 1.14 |
| Liver | 1050 | 1050 | 4.50 | 6.00 | 1.14 |

**Table 2.** Temperature field parameters.[24,25]

| Medium | $c_{\mathrm{t}}$/J·K$^{-1}$·kg$^{-1}$ | $k_{\mathrm{t}}$/W·m$^{-1}$·K$^{-1}$ |
|---|---|---|
| Water | 4180 | 0.50 |
| Skin | 3300 | 0.45 |
| Fat | 3700 | 0.50 |
| Liver | 3700 | 0.50 |

Figure 1 shows the model of our numerical calculations. The parameters used in the simulation are shown in the illustration, including the following: $a_1 = 50$ mm, $a_2 = 22.5$ mm, $r = 100$ mm, $r_1 = 3$ mm, $r_2 = 17$ mm, $r_3 = 20$ mm, $f = 1.26$ MHz, and $p_0 = 100$ kPa.

To guarantee the correctness of the simulation model, we first compared the simulation results with actual values reported in the literature.[26] Figure 3 shows the distribution of the axial temperature rise in the tissue for an outer and inner radii of the focusing transducer of 50 and 25 mm, a geometric focal length of 80 mm, a frequency of 0.9 MHz, an initial sound pressure of 173.2 kPa, and a radiation time of 6 s. The distance between the transducer and the surface of the liver is 70 mm and the region between the transducer and the liver is filled with water. The maximum temperature rise is $\sim 51.4$ °C. Compared with the results in Ref. [26] where the maximum temperature rise is $\sim 52$ °C after 6 s, the simulation results of the two models are essentially identical, which validates our numerical algorithm.

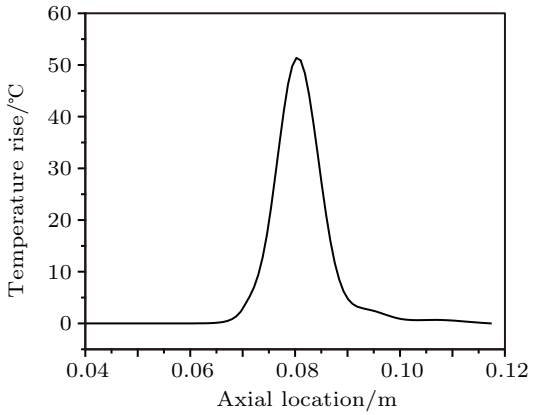



**Fig. 3.** Distribution of axial temperature rise.

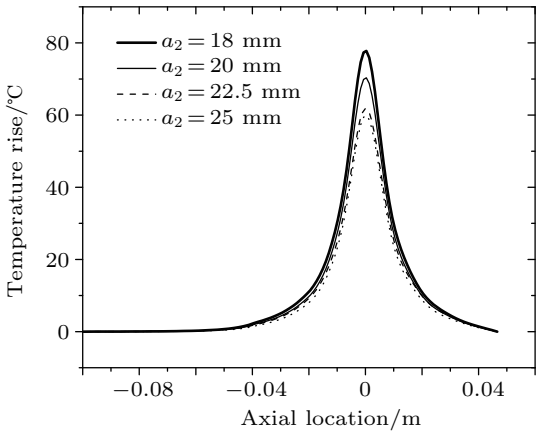



**Fig. 4.** Axial temperature rise at different geometric inner radii.

Figure 4 shows the tissue temperature rise induced by the annular focused transducer with changes in the inner radius of the transducer. When the inner radius of the focused transducer increases the maximum temperature rise decreases. This can be interpreted as follows: when the inner radius increases, the sound energy from the transducer surface decreases, and therefore the temperature of the tissue decreases. Figure 5 shows the maximum liver temperature and skin temperature rise at different geometric inner radii. It indicates that while the inner radius increases, the temperature rise of the skin slightly decreases. In other words, the influence of the inner radius on the temperature rise of skin can be ignored.

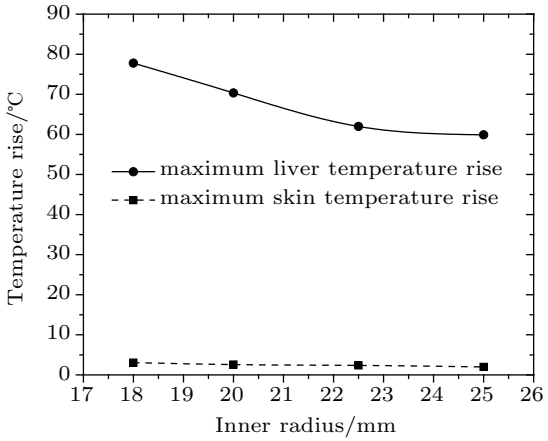



**Fig. 5.** Maximum liver temperature and skin temperature rises at different geometric inner radii.

Different geometric focal lengths from 0.08 to 0.15 m were used to calculate the temperature field for the annular focused transducer with the other parameters the same as considered previously. Figures 6 and 7 show the comparative results, indicating that both the liver temperature and skin temperature rises increased with increasing focal length. When the geometric focal length increases from 0.08 to 0.15 m, the half-aperture angle decreases from 38.7° to 19.5°, while the radii of the focused transducer are unchanged, and both the effective radiation area and sound energy are essentially unchanged. Owing to the increase in the geometric focal length, the focus area is smaller and acoustic energy per unit area of the focus area increases. Therefore, the temperature of the focus area increases with increasing geometric focal length. The maximum temperature rises of the skin and liver increase by $\sim 9$ °C and $\sim 35$ °C, respectively, while the focal length increases from 0.08 to 0.15 m. The growth rate is considerable, indicating that the focal length of the transducer also influences the rise in skin temperature. Therefore, when selecting the focal length, the maximum temperature rise of the skin needs to be simultaneously considered, while taking into account the maximum temperature rise of the target tissue.

Different transducer frequencies are used to study the relationship between the temperature rise and frequency. Figure 8 shows that the maximum liver temperature rise first increased before decreasing while the frequency increased, and

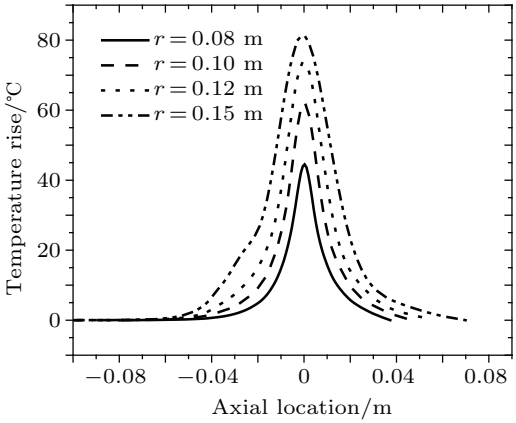



**Fig. 6.** Axial temperature rise at different geometric focal lengths.

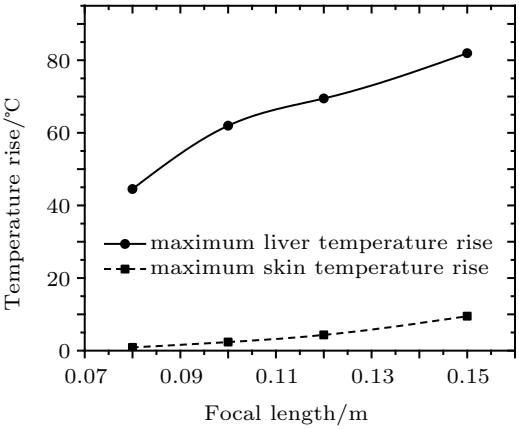



**Fig. 7.** Maximum liver temperature and skin temperature rises at different geometric focal lengths.

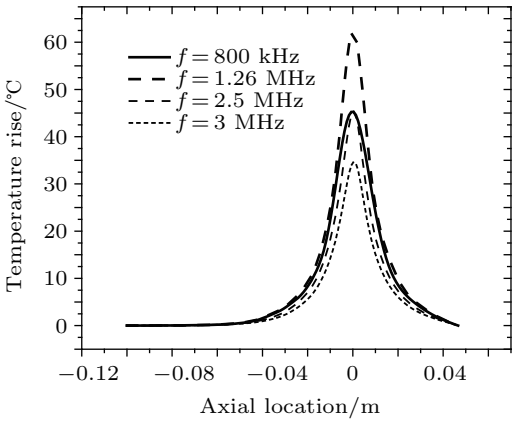



**Fig. 8.** Axial temperature rise at different frequencies.

the focus area becomes smaller. In other words, increasing the frequency improves the focusing ability of the transducer when the other parameters are unchanged. The influence of the frequency on the temperature rise is dependent on $Q_v$ according to Eqs. (8) and (10). $Q_v$ is related to the sound absorption coefficient ($\alpha$) and the sound intensity (I). For an increase in frequency, the sound absorption coefficient increases and the sound intensity decreases. The sound absorption coefficient takes priority firstly, so the temperature rise increases while the frequency increases. When the contribution of the sound absorption coefficient and sound intensity to $Q_v$ are balanced, the temperature rise reaches a maximum. The sound intensity then takes priority, and the temperature rise decreases and frequency increases. This indicates that choosing a suitable frequency is essential for the efficiency of the treatment. Figure 9 also shows the influence of the frequency on the temperature rise of skin and is negligible.

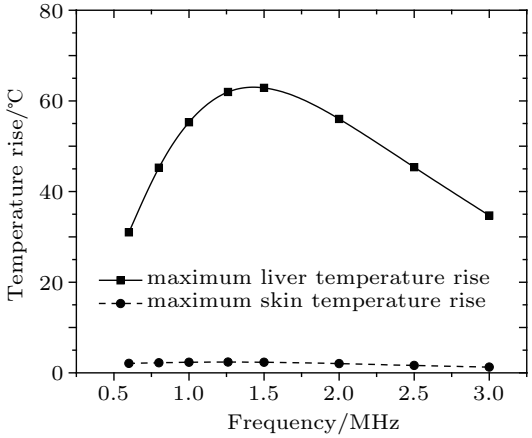



**Fig. 9.** Maximum liver temperature and skin temperature rises at different frequencies.

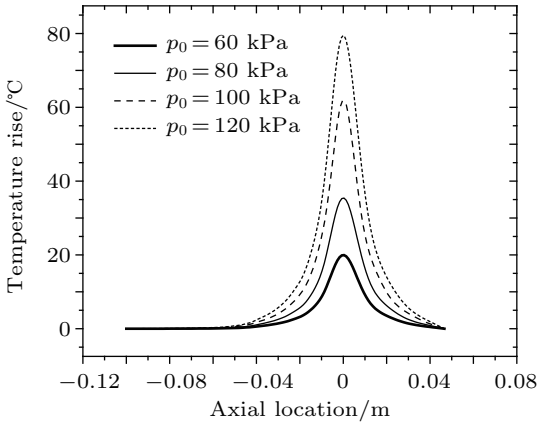



**Fig. 10.** Axial temperature rise at different sound pressures.

In order to improve the efficiency of an HIFU using an annular focused transducer, it is necessary to study the relationship between the sound pressure and temperature rise. The sound pressure is changed from 60 to 120 kPa and the other parameters of the focused transducer are constant. From Fig. 10, it is evident that the greater the power, the greater the temperature rise. The growth rate of the highest temperature rise is initially similar to exponential growth and then tends to be gradual, as shown in Fig. 11. Moreover, the temperature rise of the skin increases by a small amount when the sound pressure increases. Increasing the sound pressure produces a greater temperature. However, in practical applications, to prevent

damage to the skin and other normal tissues the sound pressure must be kept below a safe threshold.

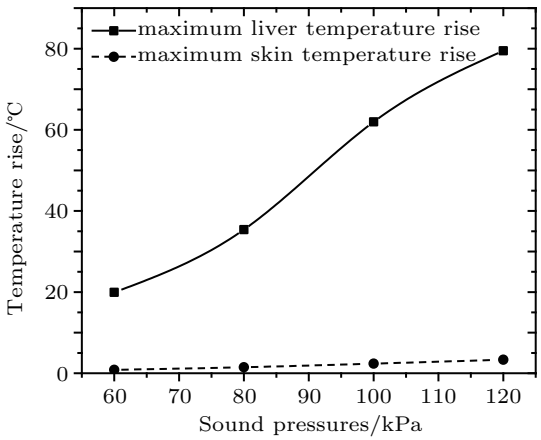



**Fig. 11.** Maximum liver temperature and skin temperature rises at different sound pressures.

## 4. Conclusion

Through numerical calculations, the influence of parameters, such as inner radius, focal length, frequency, and sound pressure, on the temperature rise in tissue induced by an annular focused transducer with a wide aperture angle were discussed. The results showed that when the geometric inner radius decreased or focal length increased, the maximum liver temperature rise increased. As the frequency increased, the maximum liver temperature rise underwent initial growth, before gradually increasing and finally decreasing. Therefore, choosing a suitable frequency is necessary for the ultrasound treatment. Increasing the focal length of the annular focused transducer also clearly leads to an increase in the maximum temperature rise of skin, so it is necessary to improve the efficiency while preventing damage to the skin. This work can provide guidance for the clinical treatment of liver cancer by an annular focused transducer.

## References

[1] Kennedy J E, TerHaar G R and Cranston D 2003 *Brit. J. Radio* **76** 590
[2] Evans K D, Weiss B and Knopp M 2007 *JDMS* **23** 319
[3] Arefiev A, Prat F, Chapelon J Y, Tavakkoli J and Cathignol D 1998 *Ultrasound Med. Biol.* **24** 1033
[4] Wang Z B, Wu F, Wang Z L, Zhang Z, Zou J Z, Liu C, Liu Y G, Cheng X, Du Y H, He Z C, Gu M L, Wang Z G and Feng R 1997 *Ultrason. Sonochem.* **4** 181
[5] McDannold N, Clement G T, Black P, Jolesz F and HynynenK 2010 *Neurosurgery* **66** 323
[6] Yoshizawa S, Ikeda T, Ito A, OtaY, Takagi S and Matsumoto Y 2009 *Med. Biol. Eng. Comput.* **47** 851
[7] Averkiou M A and Cleveland R O 1999 *J. Acoust. Soc. Am.* **106** 106102
[8] Fry F J 1958 *Am. J. Phys. Med. Rehab.* **37** 152
[9] Diederich C J and Hynynen K 1999 *Ultrasound Med. Biol.* **25** 871
[10] Liu X Z, Li J L, Chang Y, Gong X F, Zhang D and Hong H X 2007 *Phys. Lett. A* **362** 50
[11] Li J L, Liu X Z, Zhang D and Gong X F 2007 *Ultrasound Med. Biol.* **33** 1413
[12] Kamakura T, Ishiwata T and Matsuda K 1999 *J. Acoust. Soc. Am.* **105** 3083
[13] Lin J X, Liu X Z, Gong X F, Ping Z H and Wu J R 2013 *J. Acoust. Soc. Am.* **134** 1702
[14] Liu X Z, Chang Y, Gong X F and Wen W C 2010 *Ultrasound Med. Biol.* **36** 1704
[15] Wang X, Lin J X, Liu X Z, Liu J H and Gong X F 2016 *Chin. Phys. B* **25** 044301
[16] Suo D J, Guo S J, Lin W L, Jiang X N and Jing Y 2015 *Phys. Med. Biol.* **60** 7403
[17] Guo S J, Jing Y and Jiang X N 2013 *IEEE Tran. Ultrason. Ferr.* **60** 1699
[18] Kujawska T, Secomski W, Byra M, Postema M and Nowicki A 2017 *Ultrasonics* **76** 92
[19] Zhang Q, Li F Q, Feng R, Xu J Y, Bai J, Wang Z B and Wang Y J 2003 *Ultrasound Med. Biol.* **29** 585
[20] Li F Q, Gong X B, Hu K, Li C Y, Xu J, Tan Q H and Wang Z B 2006 *Chi. J. Usg.* **15** 943
[21] Xia R M 2003 *J. Comput. Acoust.* **11** 47
[22] Lucas B G and Muir T G 1982 *J. Acoust. Soc. Am.* **72** 1289
[23] Pennes H H 1948 *J. Appl. Physiol.* **1** 93
[24] Hallaj I M, Cleveland R O and Hynynen K 2001 *J. Acoust. Soc. Am.* **109** 2245
[25] Duck F A 1990 *Physical Properties of Tissues: A Comprehensive Reference Book* (London: Academic Press) pp. 834–834
[26] Chen X R, Wang S L, Zhang X J, Li Z H and Guan X Q 2012 *Acta. Biophys. Sin.* **28** 73